Dynamic effective anisotropy: Asymptotics, simulations and microwave experiments with dielectric fibres

Lauris Ceresoli[1], Redha Abdeddaim[1], Tryfon Antonakakis[2], Ben Maling[2], Mohamed Chmiaa[1], Pierre Sabouroux[1], Gérard Tayeb[1], Stefan Enoch[1], Richard V. Craster[2], and Sébastien Guenneau[1,*]

[11] *Aix-Marseille Université, CNRS, Centrale Marseille, Institut Fresnel, 13013 Marseille, France*

[2] *Department of Mathematics, Imperial College London, London SW7 2AZ, UK**

We investigate dynamic effective anisotropy in photonic crystals (PCs) through a combination of an effective medium theory, which is a high-frequency homogenisation (HFH) method explicitly developed to operate for short-waves, numerical simulations and through microwave experiments. The HFH yields accurate prediction of the effective anisotropic properties of periodic structures when the typical wave wavelength is on the order of the array pitch, specifically we investigate a square array of pitch 2 cm consisting of dielectric rods of radius 0.5 cm and refractive index $n = \sqrt{6}$ within an air matrix. This behaves as an effective medium, with strong artificial anisotropy, at a frequency corresponding to a flat band emerging from a Dirac-like point in transverse magnetic (TM) polarization (i.e. longitudinal electric field parallel to the rod axis); highly-directive emission for an electric source placed inside this PC is predicted at critical frequencies. The artificial anisotropy can be shown to coincide with a change of character of the underlying effective equation from isotropic to unidirective, with markedly different values for the effective equation tensor. In transverse electric polarization, we note an even more radical change of character of the underlying effective equation from elliptic to hyperbolic near a frequency at which an inflection point occurs in dispersion curves. Delicate microwave experiments are performed in both polarizations for such a PC consisting of 80 rods and demonstrate that a directive emission in the form of a + (resp. an X) is indeed seen experimentally at the predicted frequency 9.5 GHz in TM polarization (resp. 6 GHz in TE polarization). These are clearly dynamic effects since in the quasi-static regime the PC just behaves as an isotropic medium.

INTRODUCTION

Over the past 25 years, many significant advances have created a deep understanding of the optical properties of photonic crystals (PCs) [1–3], which are dielectric periodic structures that prohibit the propagation of light, or allow it only in certain directions at certain frequencies, or localise light in specified areas. However, PCs not only display photonic band gaps but more generally share a complex photonic band structure displaying strong dispersion and anisotropy [4, 5] allowing for a number of interesting optical phenomena such as superprism [6], self-collimation [7, 8] and ultrarefractive [9] features. Applied mathematicians try to capture the essence of the physical phenomena within a PC through homogenization theories [10]. Unfortunately these are usually limited to the quasi-static regime and therefore cannot tackle the dynamic effects listed above. A great advantage of homogenization, or effective medium, theories is that they replace a possibly complicated microstructure with a single effective medium, with the relevant physical properties encapsulated by effective parameters in some "average" sense. Recently, [11], a dynamic homogenization theory has been developed entitled high-frequency homogenization (HFH) that claims to overcome this limitation of homogenization to low frequencies. The HFH theory makes various predictions regarding dynamic anisotropy, which are captured through changes in the coefficients of a frequency-dependent tensor. Our aim is to explore one such effect and to compare with experiments thereby validating HFH as an efficient design and interpretation tool.

To distinguish HFH within the broader area of asymptotic methods, it focuses attention on the physics within a supercell of sidelength L, which is the long-scale, and captures the fine details of fields oscillations inside an elementary cell of sidelength $2l$ much smaller than L [11]. In contrast with classical homogenization theories [10], the wavelength need not be large compared to l in order to perform the asymptotic analysis, as the small parameter $\eta = l/L$ only requires the supercell to be much larger than its constituting elementary cells.

In this article, we choose a specific photonic crystal arrangement, then apply the asymptotic theory to gain insight into how the anisotropy arises for an electric and a magnetic source placed in its center. The theory gives a prediction of both the specific frequency and the shape of the mode in question in transverse magnetic (TM) and transverse electric (TE) polarizations, which is then investigated through experiment. The experiments confirm directive emission in the form of an + (resp. an X) in TE (resp. TM) polarization at a frequency corresponding to a flat band emerging from a Dirac point in TE (resp. an inflection point in TM) polarization. We are unaware of similar TE and TM experiments for a PC with dielectric fibers.

MATHEMATICAL SETUP OF THE PHYSICAL PROBLEM

We consider a PC of dielectric fibres assembled as shown in Fig. 1. We use rectangular Cartesian coordinates in space, $(x_1, x_2, x_3) = (\mathbf{x}, x_3)$, with $\mathbf{x}$ the transverse coordinates and x_3 taken along the fibre axis (x_3 is the axis perpendicular to the woodplates in Fig. 1).

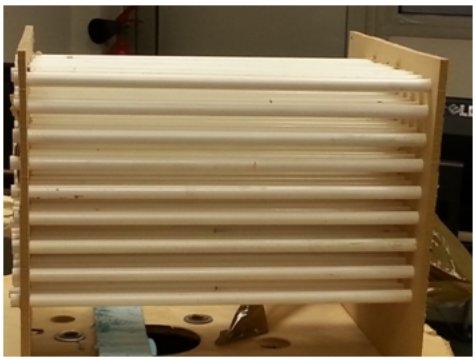

Figure 1: Photo of the dielectric photonic crystal which consists of 80 parallel dielectric rods inserted in a square array of holes drilled in hardwood plates on either sides.

Transverse magnetic (TM) polarization

In this coordinate system it is natural to work in transverse magnetic polarization in terms of the longitudinal electric field $\mathbf{E}(\mathbf{x}) = (0, 0, E_3(\mathbf{x}))\exp(-i\omega t)$ where ω is the angular wave frequency. This time dependence is assumed understood and suppressed henceforth. In this TM polarisation time-harmonic solutions of Maxwell's equations satisfy a Helmholtz equation [3]:

$$(\nabla^2 + \omega^2 \varepsilon_r \varepsilon_0 \mu_0) E_3 = 0 \,, \tag{1}$$

where ε_r is the spatially varying relative dielectric permittivity and $\varepsilon_0\mu_0 = c^{-2}$ with c the speed of light in vacuum. Moreover, $\nabla^2 = \partial^2_{x_1} + \partial^2_{x_2}$ is the Laplacian in transverse coordinates.

If we consider an infinite doubly periodic medium upon a square lattice then this equation can be supplied with Floquet-Bloch boundary conditions at the edges of a square periodic cell, with sidelength say $2l$, given by

$$\begin{array}{l} E_3(l, x_2) = e^{\mathrm{i}\kappa_1} E_3(-l, x_2), \\ \partial_{x_1} E_3(l, x_2) = e^{\mathrm{i}\kappa_1} \partial_{x_1} E_3(-l, x_2), \\ E_3(x_1, l) = e^{\mathrm{i}\kappa_2} E_3(x_1, -l), \\ \partial_{x_2} E_3(x_1, l) = e^{\mathrm{i}\kappa_2} \partial_{x_2} E_3(x_1, -l). \end{array} \tag{2}$$

This is an essential step in constructing the dispersion curves that characterise wave propagation through the medium and yields the so-called stop band diagrams [3] as, for instance, shown in Figure 2. Equations (2) involve the Bloch wave-vector $\boldsymbol{\kappa} = (\kappa_1, \kappa_2)$ characterising the phase-shift as one moves from one cell to the next. Restricting our analysis to a piecewise constant dielectric permittivity describing a square array of circular dielectric rods, the Helmholtz equation (1) needs to be solved in each homogeneous phase within the periodic cell. In addition to the Floquet-Bloch conditions (2), one has to ensure that E_3 and its Neumann derivative $\nabla E_3 \cdot \mathbf{n}$ are continuous across the circular boundary, where $\mathbf{n}$ is the outward unit normal to the boundary.

Transverse electric (TE) polarization

In the transverse electric polarization, we now consider the longitudinal magnetic field $\mathbf{H}(\mathbf{x}) = (0, 0, H_3(\mathbf{x}))\exp(-i\omega t)$ as the unknown and Maxwell's equations lead to:

$$(\nabla^T \varepsilon_r^{-1} \nabla + \omega^2 \varepsilon_0 \mu_0) H_3 = 0 \,, \tag{3}$$

where $\nabla^T = (\partial_{x_1}, \partial_{x_2})$ denotes the transpose of the gradient in transverse coordinates.

The Floquet-Bloch boundary conditions at the edges of the periodic cell are as in Equation (2) with the unknown E_3 replaced by H_3. However, in the TE polarization one has to ensure that H_3 and $\varepsilon_r^{-1}\nabla H_3 \cdot \mathbf{n}$ are continuous across the circular boundary, where $\mathbf{n}$ is the outward unit normal to the boundary. The latter boundary conditions are slightly more involved than for the TM case.

HIGH FREQUENCY HOMOGENIZATION

We now describe the essential steps behind the effective medium theory (HFH) we use; the general development is in [11] with an application to the TM electromagnetic case in [17] for a doubly periodic array of infinite conducting fibres (Dirichlet inclusions) and in [12] for three-phase checkerboards.

In the present paper we address the case of dielectric fibres in both TE and TM polarization. The basic idea is that the behaviour at the edges of the Brillouin zone, where standing waves occur, encodes the information about the local behaviour and the multiple scattering between the cylinders. This local behaviour is then modulated by a function on the long-scale that satisfies an effective equation. All of this can be made rigorous and the mathematical theory is in [11, 17]. In brief, we consider a square cell, of size l, that repeats to fill a supercell, of size L, which encompasses $(L/l)^2$ cells within the transverse plane. The discrepancy between scales is used to create a multiple scales approach and we introduce microscopic and macroscopic variables $\boldsymbol{\xi} = \mathbf{x}/l$ and $\mathbf{X} = \mathbf{x}/L$ respectively and treat $\boldsymbol{\xi}, \mathbf{X}$ as being independent. The longitudinal electric field $E_3(\mathbf{x})$ is written as

$E_3(\mathbf{X},\boldsymbol{\xi})$, and then expanded in terms of a small parameter $\eta = l/L \ll 1$, so

$$E_3(\mathbf{X},\xi) = E_3^{(0)}(\mathbf{X},\xi) + \eta E_3^{(1)}(\mathbf{X},\xi) + \eta^2 E_3^{(2)}(\mathbf{X},\xi) + ... \tag{4}$$

, the longitudinal magnetic field is similarly expanded as $H_3(\mathbf{X},\boldsymbol{\xi}) = H_3^{(0)}(\mathbf{X},\xi) + ...$, and the frequency as $\omega^2 = \omega_0^2 + \eta\omega_1^2 + \eta^2\omega_2^2 + \ldots$. The leading order solution $E_3^{(0)}(\mathbf{X},\xi)$ (resp. $H_3^{(0)}(\mathbf{X},\xi)$) turns out to be the standing wave frequency ω_0 and proportional to the associated Bloch eigensolution on the short-scale which we call $U_0^E(\boldsymbol{\xi})$ (resp. $U_0^H(\boldsymbol{\xi})$). This standing wave frequency, which can be high, and the eigensolution, which can oscillate rapidly, are easily found from the usual Bloch analysis that leads to the dispersion curves. The leading order electric and magnetic fields are then given as

$$\begin{aligned} E_3^{(0)}(\mathbf{x},\boldsymbol{\xi}) &= f_0^E(\mathbf{X})U_0^E(\boldsymbol{\xi}) \,, \\ H_3^{(0)}(\mathbf{x},\boldsymbol{\xi}) &= f_0^H(\mathbf{X})U_0^H(\boldsymbol{\xi}) \,, \end{aligned} \tag{5}$$

so the short-scale, potentially highly oscillatory, field $U_0^E(\boldsymbol{\xi})$ (resp. $U_0^H(\boldsymbol{\xi})$) is modulated by a long-scale function $f_0^E(\mathbf{X})$ (resp. $f_0^H(\mathbf{X})$). The key point of the analysis of [11] is to show that this long-scale field satisfies an effective partial differential equation posed entirely on the long-scale:

$$T_{ij}^{\alpha}\frac{\partial^2}{\partial X_i \partial X_j} f_0^{\alpha} + \omega_2^2 \varepsilon_0 \mu_0 f_0^{\alpha} = 0 \,, \quad \text{for} \quad i,j = 1,2. \tag{6}$$

for $T_{ij}^{\alpha} = t_{ij}^{\alpha}(\int_S b^{\alpha}(U_0^{\alpha})^2 dS)^{-1}$. Here $\alpha = E$ in TM polarization, $\alpha = H$ in TE polarization and $b^E = 1$, $b^H = \varepsilon_r$. Furthermore, t_{ij}^{α}'s are given by annex problems set on the periodic cell with diagonal entries

$$\begin{aligned} t_{ii}^{\alpha} &= \int_{-l}^{l}\int_{-l}^{l} a^{\alpha}(U_0^{\alpha})^2 d\xi_1 d\xi_2 \\ &+2\int_{-l}^{l}\int_{-l}^{l} a^{\alpha}\partial_{\xi_i} U_{1_i} U_0^{\alpha} d\xi_1 d\xi_2 \\ &+\int_{-l}^{l}\int_{-l}^{l} \partial_{\xi_i} a^{\alpha} U_{1_i} U_0^{\alpha} d\xi_1 d\xi_2, \end{aligned} \tag{7}$$

and off-diagonal entries

$$\begin{aligned} t_{ij}^{\alpha} &= 2\int_{-l}^{l}\int_{-l}^{l} a^{\alpha}\partial_{\xi_i} U_{1_j} U_0^{\alpha} d\xi_1 d\xi_2 \\ &+\int_{-l}^{l}\int_{-l}^{l} \partial_{\xi_i} a^{\alpha} U_{1_j} U_0^{\alpha} d\xi_1 d\xi_2 \quad \text{for} \quad i \neq j \,, \end{aligned} \tag{8}$$

where $a^E = \varepsilon_r^{-1}$ and $a^H = 1$, in TM and TE polarization, respectively. It should be noted that the vector field $\mathbf{U_1}(\boldsymbol{\xi})$ in (8) comes from the first term in the ansatz (4), see e.g. [11],

$$E_1(\mathbf{X},\boldsymbol{\xi}) = f_1^E(\mathbf{X})U_0^E(\boldsymbol{\xi};\Omega_0) + \nabla_{\mathbf{X}} f_0^E(\mathbf{X}) \cdot \mathbf{U_1}^E(\boldsymbol{\xi}), \tag{9}$$

when $\alpha = E$ and likewise when $\alpha = H$ with $H_1(\mathbf{X},\boldsymbol{\xi})$.

The short-scale is completely encoded within the tensor T_{ij}^{α}, which takes numerical values dependent upon the geometry, material parameters and standing wave frequency; crucially it does depend upon ω_0 (which obviously is different in TE and TM polarizations) and so captures dynamic effects. Equation (6) encapsulates the dynamic effective anisotropy of the photonic crystal through the tensor T_{ij}^{α}. The detailed derivation of (6) can be found in [11, 17] and an interpretation of the T_{ij}^{α} in terms of effective media is in [12]. There are some subtleties associated with repeated eigenvalues which occur when dispersion branches cross at a standing wave frequency. In such cases (6) requires modification as detailed in [17]. Note that there is no summation over repeated indexes for the t_{ii} and the t_{ij}. The structure of the tensor depends upon the boundary conditions of the inclusions, the results here, for instance, are different in TE and TM cases and also from those of the Neumann and Dirichlet [17] cases.

It should be noted that the tensor T_{ij}^{α} can have negative values, or components, and it allows one to interpret and, even more importantly, predict changes in behaviour of the effective equation (6) when specific physical effects might occur. There is notably a possible transition to hyperbolic behaviour [17], which is reminiscent of recent work on hyperbolic metamaterials [18–24].

FEM VERSUS HFH DISPERSION CURVES FOR STRUCTURED DIELECTRIC FIBRES

We focus on a specific case: a dielectric rod of relative permittivity 6 and radius 0.5 cm is surrounded by air in a square cell of sidelength $2l = 2$ cm. This elementary cell is a good model for the PC shown in Fig. 1. For Floquet-Bloch conditions to be applied on its sides, we imagine an infinite medium made from this square cell periodically repeated indefinitely. This enables us to draw band diagrams which can display interesting features such as vanishing or negative group velocity.

TM polarization

Fig.2 shows the resulting dispersion curves computed with finite elements (solid curves) and those obtained from HFH (dashed curves) in transverse magnetic polarization. We notably observe some missed crossing between the third and the first two dispersion curves at the Γ point, which is reminiscent of Dirac points in arrays of constrained (Dirichlet) points [17]. We note that arrays of thin metal wires have been studied back in the 90's in conjunction with zero-frequency band gaps and non-commuting limits [25].

The HFH curves result from asymptotics around the points Γ, X and M, and so are highly accurate there,

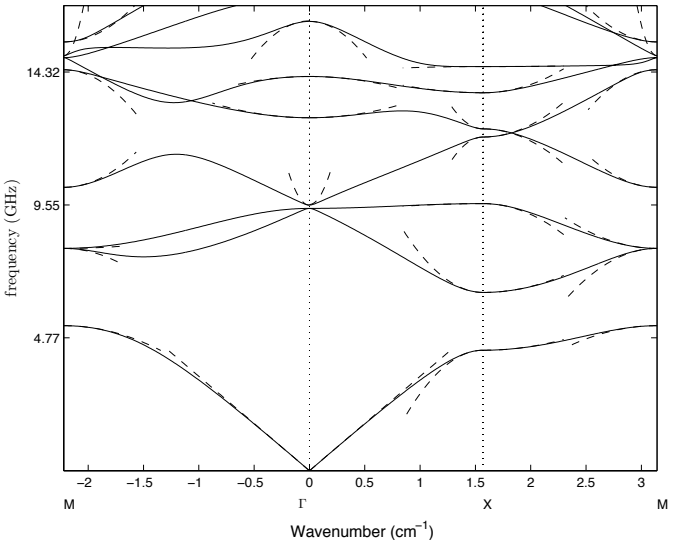

Figure 2: Floquet-Bloch dispersion curves for a circular dielectric inclusion of radius $r = 0.5$cm and relative permittivity 6, surrounded by air in a periodic cell of sidelength $2l = 2$cm in TM polarization. Solid curves are from FEM and dashed curves from the asymptotic HFH.

which in itself is a useful cross-verification of the effective medium methodology. Incidentally, one can extend the domain of validity by working with an elementary cell of 2×2 cylinders and then one gets asymptotics along the middle of, say, the path ΓM (see [17]). At this point some brief explanation is required of the wavenumber axis. In wavenumber space the Brillouin zone is a square, but the symmetry of the cell allows us to treat an irreducible Brillouin zone, which is a triangle joining the points $\Gamma = (0,0)$, $X = (\pi/2, 0)$ and $M = (\pi/2, \pi/2)$. As is conventional we show the dispersion curves for wavenumbers taken around the edge of this triangle $\Gamma X M$.

From Fig.2 we see that a photonic band gap exists in TE polarization, and this is known to allow for microcavity effects if one makes a defect in the photonic crystal [14]. Further effects can also be predicted from the dispersion curves, for instance one can achieve slow light [15] effects at symmetry points of the Brillouin zone, where the slope of the dispersion curves is zero. The behaviour at the edges of the Brillouin zone is key to interpreting the band diagram.

TE Polarization

There is a radical change in the band spectrum when we look at the other polarization case. From Fig.3 we note that the stop band is no longer present in TE polarization. The Dirac cone is no longer seen in this polarization. So, at first sight, one might say the TM polarization seems to be more prone to interesting physical effects. However, we shall see in the sequel that the PC behaves like a hyperbolic-type metamaterial near the frequency 6 GHz at which an inflection point exists in TE polarization.

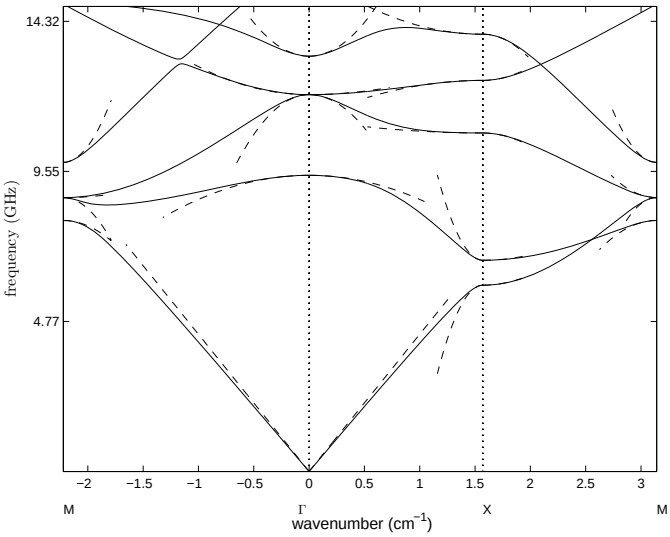

Figure 3: Floquet-Bloch dispersion curves in TE polarization for same PC parameters as in Fig. 2. Solid curves are from FEM and dashed curves from the asymptotic HFH.

FEM VERSUS HFH MODES FOR PHOTONIC CRYSTAL

It is interesting to approximate the dispersion curves with HFH theory. The resulting curves are shown as dotted lines in Fig. 2 and 3. Classical homogenization can only capture the effective linear curves near the Γ point, whereas HFH neatly approximate solid curves computed with finite elements even in the stop band range of frequencies. Tiny departure from solid curves away from the Γ, X and M points, can be resolved by considering higher-symmetry points in the first Brillouin zone [17].

TM polarization

The effective medium methodology allows us to say more about the band-gap edges modes; it transpires that there is a whole class of exotic effective behaviours to be gained with slow modes, and the T_{ij} coefficients encode this information. For instance, near the X symmetry point in Fig.2, one gets a mode (the third mode at 9.5 GHz), which displays strong dynamic anisotropy as $|T_{11}| \ll |T_{22}|$ with $T_{12} = T_{21} = 0$; the values are $T_{11} = -0.1548$, $T_{22} = -1.7773$.

This anisotropy leads to the highly directive radiative pattern observed in the full computations of Fig.4(c) reminiscent of self-collimation in scattering problems with

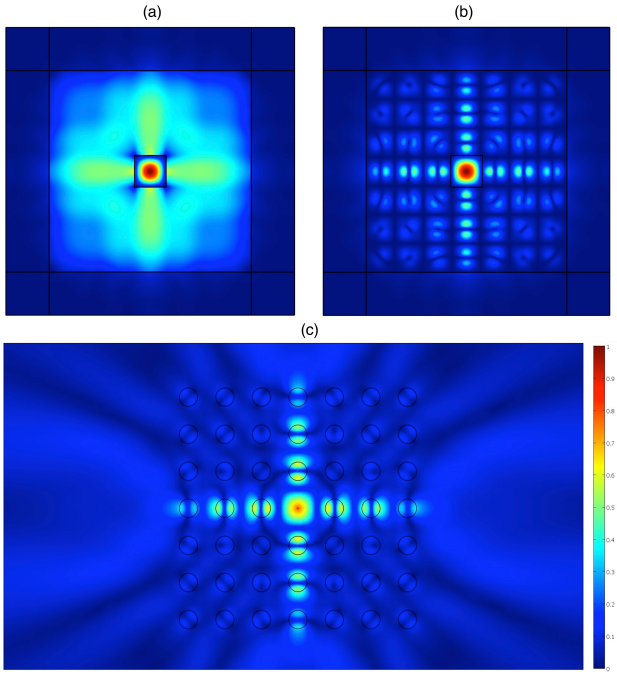

Figure 4: The modulus of the longitudinal electric field, E_3, for a line source at 9.5GHz placed in the centre of a PC with properties as in Fig. 2: Panels (a) and (b) show Comsol Multiphysics computations using the effective medium (HFH) theory where the T_{ij} are for the 3rd mode at X which are $T_{11} = -0.1548$, $T_{22} = -1.7773$, $T_{12} = T_{21} = 0$. Panel (a) shows only the long-scale component $|f_0|$ and (b) shows the leading order asymptotic solution $|E_3^{(0)}(\mathbf{x}, \boldsymbol{\xi})| = |f_0^E(\mathbf{x})U_0^E(\boldsymbol{\xi})|$. In both panels the computational region is surrounded by a layer of perfectly matched layers (to prevent artificial reflections due to the truncation of an infinite domain) which is outside the lines in these panels. Panel (c) shows the full Comsol simulation using the Helmholtz equation (1). Clearly the agreement of asymptotic and full computation is excellent both qualitatively and quantitatively. Color scale is linear.

photonic crystals. Computations using the effective theory in Fig.4(b) are remarkably accurate, and the magnitude of the long-scale modulation function f_0 is shown in Fig.4(a). One can accurately predict using the asymptotic theory that this highly directional behaviour will exist from the evident anisotropy of the tensor T_{ij}. Another key advantage of having an effective theory, valid for high frequencies, is that the computations for the effective equation are an order of magnitude faster than those of full computations for the microstructured medium.

TE polarization

It is worth noting that self-collimating is not the only directional anisotropy that can arise. In the other polarization case, we achieve an X-shaped emission when $T_{11}T_{22} < 0$, in which case the effective equation (6) describes that of a hyperbolic metamaterial [16]. Here again HFH reproduces almost perfectly the emission of a magnetic source inside the PC computed with finite elements. This striking effect is shown in Fig.5. For simple geometries some gap-edge asymptotics of defect modes can also be derived using a Green's function approach [13].

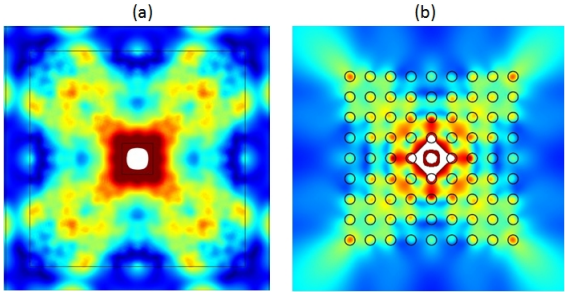

Figure 5: The modulus of the longitudinal magnetic field, H_3, for a line source at 5.9GHz placed in the centre of a PC with properties as in Fig. 2: Panels (a) and (b) show Comsol Multiphysics computations using the effective medium (HFH) theory where the T_{ij} are for the 3rd mode at X which are $T_{11} = -8.6656$, $T_{22} = 0.9209$, $T_{12} = T_{21} = 0$. Panel (a) shows only the long-scale component $|f_0|$ and (b) shows the leading order asymptotic solution $|H_3^{(0)}(\mathbf{x}, \boldsymbol{\xi})| = |f_0^H(\mathbf{x})U_0^H(\boldsymbol{\xi})|$. In both panels the computational region is surrounded by a layer of perfectly matched layers (to prevent artificial reflections due to the truncation of an infinite domain) which is outside the lines in these panels. Panel (c) shows the full Comsol simulation using the Helmholtz equation (1). Clearly the agreement of asymptotic and full computation is excellent both qualitatively and quantitatively. Color scale is linear.

MICROWAVE EXPERIMENTS

Now that we have a design tool, HFH, at our disposal we can use it interactively with experiments to find the key operating frequencies and material parameters for directivity, amongst other effects. The predictions described thus far are now explored with a novel set of experiments. In Fig.6 and Fig. 7, we show experimental measurements for the photonic crystal designed and characterized at the Institut Fresnel. The structure shown in Fig.1 is a PC of square symmetry made of 80 dielectric rods (a 9×9 array with the central rod removed). These rods consist of alumina powder and synthetic resin, they are 0.5 cm in radius and 300 mm long, respectively, and their relative permittivity was shown to be equal on average to 6 (with up to 5 per cent of inaccuracy) in [14]. This is the experimental analogue of that used in the theory, except that the computations for Fig.4 are planar, corresponding to the limiting case of infinitely long fibres, whereas the experiments are three-dimensional; hence the slight discrepancy in Fig.6 (resp. Fig.7) versus those of Fig.4 (resp. Fig.5). Nonetheless, the directional anisotropy found in the experiments is very clear.

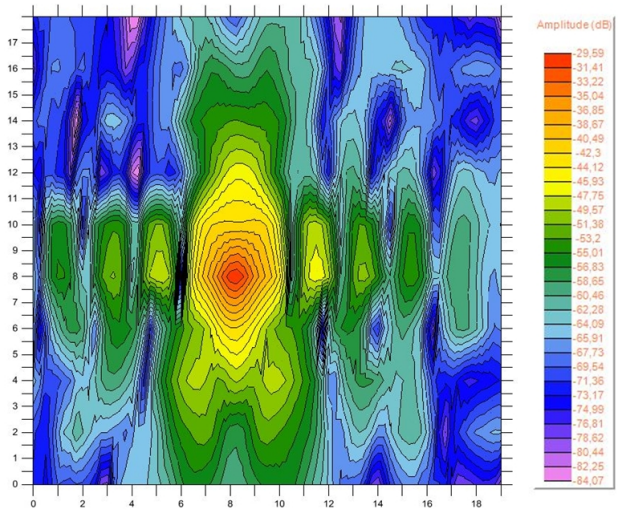

Figure 6: Result of microwave experiments for an electric source (TM polarization) at 9.5 GHz placed in the center of the PC. Color scale is in dB.

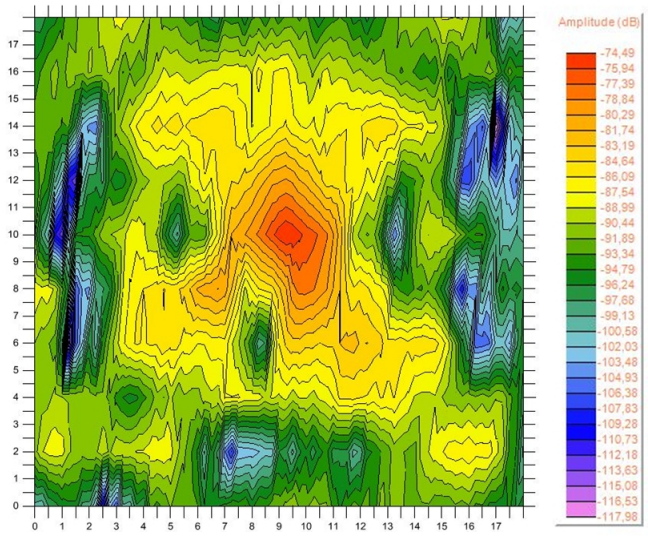

Figure 7: Result of microwave experiments for a magnetic source (TE polarization) at 5.9 GHz placed in the center of the PC. Color scale is in dB.

Fig. 4 and Fig. 6 allow for numerical and experimental comparisons of the modulus of the x_3 component of the electric field, $\mid \Re(E_3) \mid$, inside the crystal. This component is carefully measured with a vectorial network analyser using a monopole probe. A small monopole antenna is located at the centre of the structure. To ensure excitation and measurement of E_3 both the emitting monopole and the probe are aligned along x_3 (the axis parallel to the fibres, see Fig. 1). Simulations and measurements are indeed in excellent agreement. The longitudinal electric field E_3 in the two scanned direction (x_1, x_2) is maximal along the central lines (horizontal and vertical), making a cross as predicted by HFH.

In the same way, Fig. 5 and Fig. 7 allow for numerical and experimental comparisons of the modulus of the x_3 component of the magnetic field, $\mid \Re(H_3) \mid$, inside the crystal. We now use a magnetic probe for excitation and measurement of H_3 with the emitting monopole and the probe aligned along x_3. Simulations and measurements are once again in excellent agreement. The longitudinal magnetic field H_3 is maximal along the diagonal lines, making an X as predicted by HFH.

CONCLUSION AND APPLICATIONS

In this article, we have experimentally tested an effective medium formulation for dielectric photonic crystals in transverse magnetic (TM) and transverse electric (TE) polarization, which is not constrained to the low-frequency limit. This is an important step as this theory is now ideally placed to play a role in practical interpretation and design. The HFH methodology captures the dynamic nature of the anisotropy through the tensor T_{ij} and unveils the dynamic anisotropy at photonic band gap edges which leads to ultra-directive emission either along the x_1 and x_2 axes (in TM polarization) or the diagonal axes (in TE polarization). In the former case the directive effect comes from an effective tensor with a vanishing eigenvalue, while in the latter case, the eigenvalues have opposite sign (hyperbolic-type effective equation). Finally, (1) and (3) can be used to model problems of pressure acoustic, or anti-plane shear, waves with the density/bulk modulus/shear modulus playing the role of the permittivity. This suggests similar ultra-directive emission could be observed with arrays of fibres in other wave areas.

R.V.C. thanks the EPSRC (UK) for support through research grant EP/J009636/1 and programme grant EP/L024926/1. P.S., R.A., S.E., S.G. acknowledge a PEPS CNRS (France) grant Cloaking Externe. S.G. is thankful for an ERC grant Anamorphism.

* Electronic address: `$^{*}$sebastien.guenneau@fresnel.fr`

[1] E. Yablonovitch, Phys. Rev. Lett. **58**, 2059 (1987).
[2] S. John, Phys. Rev. Lett. **58**, 2486–2489 (1987).
[3] J.D. Joannopoulos, S.G. Johnson, J.N. Winn, and R.D. Meade, *Photonic Crystals, Molding the Flow of Light* (Princeton University Press, Princeton, 2008).
[4] P. St. J. Russell, Appl. Phys. B **39**, 231–246 (1986).
[5] R. Zengerle, J. Mod. Optics **34**, 1589–1617 (1987).
[6] H. Kosaka, T. Kawashima, A. Tomita, M. Notomi, T. Tamamura, T. Sato, and S. Kawakami, Phys. Rev. B **58**, R10096–10099 (1998).
[7] H. Kosaka, T. Kawashima, A. Tomita, M. Notomi, T. Tamamura, T. Sato, and S. Kawakami, Appl. Phys. Lett. **74**, 1212–1214 (1999).

[8] D.N. Chigrin, S. Enoch, C.M. Sotomayor Torres and G. Tayeb, Opt. Express **11**(10), 1203–1211 (2003).
[9] B. Gralak, S. Enoch, and G. Tayeb, J. Opt. Soc. Am. A **17**, 1012 (2000).
[10] G.W. Milton, *The Theory of Composites* (Cambridge University Press, Cambridge, 2002).
[11] R.V. Craster, J. Kaplunov, and A.V. Pichugin, Proc. R. Soc. A **466,** 2341–2362 (2010).
[12] R. V. Craster, J. Kaplunov, E. Nolde and S. Guenneau J. Optical Society America A **28**, 1032–1040 (2011).
[13] K.B. Dossou, R.C. McPhedran, L.C. Botten, A.A. Asatryan, and C.M. de Sterke, Opt. Express **15,**(8), 4753–4761 (2007).
[14] P. Sabouroux, G. Tayeb, and D. Maystre Optics Comm. **160,** 33–36 (1999).
[15] A. Figotin, and I. Vitebskiy, W. Rand. Comp. Med. **16,** 293–382 (2006).
[16] A. Poddubny, I. Iorsh, P. Belov, and Y. Kivshar, Nat. Photonics **7,** 948–957 (2013).
[17] T. Antonakakis, R.V. Craster, and S. Guenneau, New J. Physics **15**(10), 103014 (2013).
[18] W. Yan, M. Wubs, and N.A. Mortensen, Phys. Rev. B **86**, 205429 (2012).
[19] D. Schurig, and D.R. Smith,
[20] Z. Jacob, L.V. Alekseyev, and E. Narimanov, Opt. Express **14**, 8247–8256 (2006).
[21] I.I. Smolyaninov, Y.-J. Hung, and C.C. Davis, Science **315**, 1699–1701 (2007).
[22] M.A. Noginov, Y.A. Barnakov, G. Zhu, T. Tumkur, H. Li, and E.E. Narimanov, Appl. Phys. Lett. **94**, 151105 (2009).
[23] L. M. Custodio, C. T. Sousa, J. Ventura, J. M. Teixeira, P. V. S. Marques, and J. P. Araujo Phys. Rev. B **85**, 165408 (2012).
[24] C.R. Simovski, P.A. Belov, A.V. Atrashchenko, and Y.S. Kivshar, Adv. Mater. **24**, 4229–4248 (2012).
[25] N.A. Nicorovici, R.C. McPhedran and L.C. Botten, Phys. Rev. Lett. **75**, 1507 (1995).